Thermal modeling for ventilated structural components using frequency response and finite difference methods and comparison with experimental data

Yuxiang Chen, A. K. Athienitis, Khaled Galal
Department of Building, Civil and Environmental Engineering, Concordia University
Montreal, QC, Canada

Abstract

Ventilated structural components, such as ventilated concrete slabs (VCS) and ventilated masonry block walls can be used to actively store and release thermal energy by passing air through their air channels. In this paper, lumped-parameter thermal models of ventilated structural components are presented. The modeling methods include frequency response and explicit finite difference. Equations for calculating the mean temperature of the air flow are provided. In the frequency response approach, discrete Fourier series in complex frequency form are used to model the boundary excitations, such as the surface temperature variation and heat flux from air flow. In the treatment of air flow, including the activation of air flow based on VCS temperature and its heat injection as internal source in the VCS, thermal network techniques such as Thévenin theorem and Y-diakoptic transform are applied. In explicit finite difference approach, the thermal behavior modeled by multi-layer dense discretization scheme is compared with that by 2-layer and 3-layer schemes. The simulation results from frequency response and explicit finite difference approaches, the comparison between them, and the comparison with experimental data are presented.

1 Introduction

Thermal energy storage (TES) with appropriate control strategies can reduce the space cooling/heating energy consumption and peak demand of buildings (Dincer 2002, Howard and Fraker 1990, Morgan and Krarti 2007). Ventilated structural components, such as ventilated concrete slabs (VCS) and ventilated masonry block walls can be used to actively store and release thermal energy by passing air through their embedded air channels (Braham 2000, Chen et al. 2010b, Howard 1986). These components can be inherent parts of buildings and they are directly in thermal contact with room space, and hence can be referred to as building-integrated thermal energy storage (BITES) systems. Their thermal behavior interacts with the building indoor environment. In order to develop a methodology and guidelines for the design and control of BITES systems, the thermal behavior of different systems has to be quantified with acceptable accuracy. Numerical modeling is necessary for this purpose but, simple yet accurate models are needed to compare the response of BITES systems for a specific building on a relative basis and to incorporate the models into whole building simulations.

Finite difference (FD) models for ventilated concrete slabs have been widely used. Zmeureanu and Fazio (1988) presented a two-dimensionally discretized model for a hollow core slab, in which the slab cores were simplified as two parallel plates with air passing between them. Winwood et al.(1997) developed a 5-node one-dimensional FD model for a hollow core slab. Storage efficiency (i.e. ratio of potential heat recovered from the air flow) is

used in this model. Barton et al. (2002) used a two-dimensional model with denser discretization for a hollow core slab.

In the frequency response (FR) approach, different kinds of models have been developed for the above methods. Ren and Wright (1998) used a 3rd order (i.e. 3 capacitance nodes) lumped-parameter model for a hollow core slab. RC (resistance and capacitance) network techniques have been widely used (Akander 2000, Davies 1982). Fraisse et al. (2006) briefly described a RC model for a ventilated massive wall. Schmidt and Jóhannesson (2002) described a modeling method using RC network for the behavior of thermal energy storage (TES) systems with heat transfer fluid flowing. The approach assumes one-dimensional heat transfer in the solid (i.e. normal to the fluid flow direction) with constant exterior boundary conditions. Both analytical and numerical methods in frequency domain are applied and their results are compared. They further extended the study to quasi-two dimensional models (Schmidt and Jóhannesson 2004).

Lumped-parameter modeling avoids the hassles needed for 2- or 3-dimensional discretization, such as the programming time and potential errors, and computational expense. In the analysis of multi-layer plate assemblies (e.g. wall/floor/ceiling) with FR approach, the temperatures and heat flux at nodes of no interest do not need to be calculated. The layers between nodes of interest can be combined and treated as one layer. The magnitude and phase angle of admittance or impedance obtained from FR approach of an assembly provides substantial insight into its thermal behavior (Athienitis 1994, Athienitis et al. 1990, Balcomb and Jones 1983). These variables can be readily used for parametric analysis and optimization design. Frequency response methods can provide significant insights into the thermal behavior of ventilated BITES systems, particularly in comparing the relative response of design alternatives without simulation. They can also be used in model based predictive control (MPC). The motivation of this paper is to develop frequency domain thermal network models for ventilated BITES systems and to compare them with finite difference models.

FR and explicit FD modeling are applied to on two kinds of VCS systems (Figure 1). VCS-a systems have air channels on one side of the slab while VCS-b systems have their hollow cores as air channels. The modeling results are compared. The modeling result for the first kind of VCS using FD is also compared with experimental data.

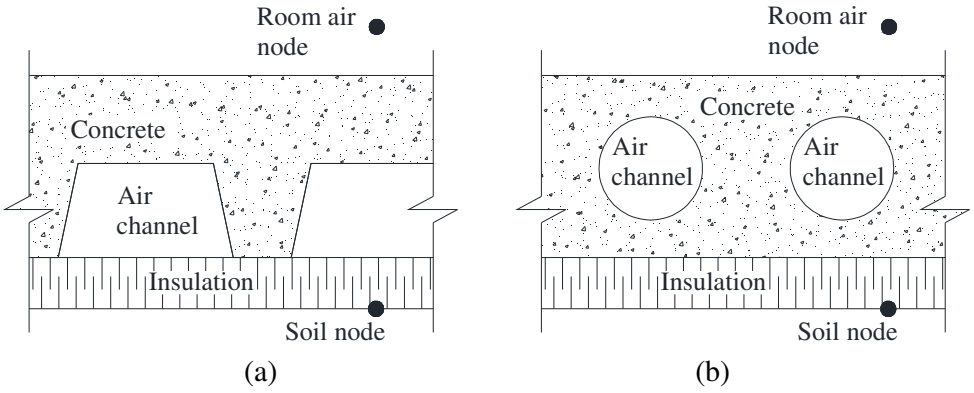

Figure 1: Two kinds of VCS studied

2 Modeling techniques

This section describes the techniques adopted in this paper for FR and explicit FD analysis of ventilated BITES systems. Heat transfer in the building components is considered one dimensional normal to the room-side surface of the slab.

Mean air temperature

The approach for obtaining the mean temperature of air flow in the air channels is as follows. For ventilated BITES systems, when the specific thermal capacity of the boundary (e.g. concrete hollow core) is much higher than that of air, it is reasonable to assume that the air channel surface temperature is uniform (Ren and Wright 1998). Chen et al. (2010b) showed that the temperature gradient of the slab along the air flow direction is not significant. Zmeureanu and Fazio (1988), Ren and Wright (1998), Charron and Athienitis (2006), and Fraisse et al. (2006) presented approaches for obtaining the local air temperature along an air path, as well as the mean air temperature. Based on their work, further equations are developed for lumped-parameter models. The equations to be presented can be used for air channels with any air path configuration, such as U configuration, and bounded with more than one surfaces.

The original heat transfer coefficients between the air flow and each of its surrounding surfaces ${}_{org\_chn}u_s$ needs to be converted to surface-area-weighted heat transfer coefficients per unit room-side surface area ${}_{eqv\_chn}u_s$. ${}_{eqv\_chn}u_s$ can be obtained by multiplying ${}_{org\_chn}u_s$ with its corresponding surface area per unit room-side area of the building component. For example, if a building component has $2\ m^2$of hollow cores per unit room-side surface area, and the CHTC (i.e. ${}_{org\_chn}u$) between the core surface and the core air is $10\ W/m^2K$. The ${}_{eqv\_chn}u$ will be 10x2=20 W/m^2K. Alternatively, ${}_{eqv\_chn}u_s$ can be obtained with Equation (1):

$$ {}_{eqv\_chn}u_s = \frac{{}_{air\_srf}p_s}{{}_{RS}Area} \tag{1} $$

given that the heat flux from air to channel surface "s", ${}_{air\_srf}p_s$, is available. Note that different ${}_{eqv\_chn}u_s$ corresponds to different channel-bounding surfaces/nodes under different air velocity (i.e. flow rate). ${}_{RS}Area$ is the room-side surface area of the ventilated component. Furthermore, ${}_{eqv\_chn}u_s$ is necessary also because FR simulation is conducted on unit area.

After equivalent heat transfer coefficients ${}_{eqv\_chn}u_s$ are obtained, the mean temperature of the air flow can now be obtained using Equation (2):

$$ {}_{mean\_air}T = {}_{bndr}T + \frac{\left({}_{inlet\_air}T - {}_{bndr}T\right)\cdot\left(1-\exp\left(-{}_{hx}c\right)\right)}{{}_{hx}c} \tag{2} $$

where ${}_{inlet\_air}T$ is the air temperature at the inlet. ${}_{bndr}T$ is the effective boundary surface temperature. ${}_{hx}c$ is a coefficient for heat exchange.

When the air channel is bounded by S surfaces

$$ {}_{bndr}T = \frac{\sum_{s=1}^{S}\left({}_{chn\_srf}T_s \cdot {}_{eqv\_chn}u_s\right)}{\sum_{s=1}^{S}\left({}_{eqv\_chn}u_s\right)} $$

$$ {}_{hx}c = {}_{RS}Area \cdot \sum_{s=1}^{S}\left({}_{eqv\_chn}u_s\right) \Big/ {}_{air}FC $$

where ${}_{chn\_srf}T$ is the surface temperature of the air channel, where ${}_{air}FC = {}_{air}F \cdot {}_{air}\rho \cdot {}_{air}c_p$ with ${}_{air}F$ being the total air flow rate.

The outlet air temperature can be obtained with Equation (3):

$$ {}_{outlet\_air}T = {}_{bndr}T + \left({}_{inlet\_air}T - {}_{bndr}T\right)\cdot\exp\left(-{}_{hx}c\right) \tag{3} $$

Techniques for FR approach

This section describes the techniques adopted in this paper for conducting FR analysis subject to periodic excitation conditions. The analysis period, P, can be of any time span, from a minute to a year, depending on the practical need (Athienitis et al. 1987). To perform FR analysis, time domain equations have to be converted to frequency domain equations. These equations include heat transfer functions and excitation functions (e.g. boundary temperatures and heat flux, and internal heat sources). The equations for FR approach in this paper are given for unit surface area.

Discrete frequency representation of excitations

In this paper, discrete Fourier series (DFS) in exponential complex frequency form are used to represent the boundary excitations, such as the surface temperature variation and heat flux from air flow. When an excitation is given in a discrete form as follows:

$$[A_i]_{1\text{xI}} = [A_{\Delta t}\ , A_{2\Delta t}\ , A_{3\Delta t}\ \ \dots\ \ A_{i\Delta t}\ \ \dots\ \ A_{I\Delta t}] \tag{4}$$

where $i = 1, 2 \dots I$, is the position index for time series values $[A_i]$. It indicates the time at which the value is sampled. Δt is the time interval of data sampling. The function of any excitation can be assumed to be even (i.e. symmetric about time origin) since one period is of interest. Its complex DFS representation can be approximated using Equation (5). See Chen (1983) and Kreyszig (2006) for more details on discrete Fourier series.

$$^{DFS}A_i \cong c_0 + 2\sum_{h=1}^{H}\left(c_h \cdot e^{jh\omega_f i\Delta t}\right) = c_0 + 2\cdot\sum_{h=1}^{H}\left(c_h \cdot e^{jh\frac{2\pi}{I}i}\right) \tag{5}$$

where $\omega_f = 2\pi/P$ is the fundamental angular frequency. P is the analysis period in seconds. $j = \sqrt{-1}$ is the imaginary unit. H is a positive integer representing how many harmonics are used in this approximation to achieve desirable accuracy.

$$c_0 = \frac{1}{I}\sum_{i=1}^{I}\left(A_i \cdot e^{-j0\frac{2\pi}{I}i}\right) = \frac{1}{I}\sum_{i=1}^{I}A_i$$

$$c_h \cong \frac{1}{I}\sum_{i=1}^{I}\left(A_i \cdot e^{-jh\omega_f i\Delta t}\right) = \frac{1}{I}\sum_{i=1}^{I}\left(A_i \cdot e^{-jh\frac{2\pi}{I}i}\right)$$

Coefficients c_0 is the mean of all the values given in time series. Each c_h calculates the magnitude (also called modulus) of the h^{th} harmonic, which has an angular frequency of $\omega_h = h \cdot \omega_f$. The summation term in Equation (5) gives the oscillation about the mean value. It is the summation of the harmonics corresponding to different frequencies. To convert the complex values back to real values

$$A_i \cong Re\{^{DFS}A_i\}$$

When an excitation is represented with a DFS (e.g. $^{DFS}A_i$ in Equation (5)), the excitation function comprises of a mean value $\bar{A} = c_0$, and different harmonics $\tilde{A}_{i,h} \cong 2 \cdot c_h \cdot e^{jh\frac{2\pi}{I}i}$, where "$-$" represents mean value, and "$\sim$" the harmonics. The final discrete response to this excitation is the summation of the response to the mean value "steady-state response" and the responses to the harmonics "oscillatory response", as given below.

$$^{FR}R(A)_i = \bar{R}(A) + \sum_{h=1}^{H}\left(\tilde{R}(A)_{i,h}\right) \tag{6}$$

where FR stands for response in complex frequency domain.

The mean value of the response is obtained using the steady-state resistance and the mean value of the excitations. Take the mean heat flow response at surface 0 of the N-layer assembly for example: ${}^{1}_{0}\bar{p} = ({}^{1}_{0}\bar{T} - {}^{N}_{l}\bar{T})/{}^{1\leftarrow N}R$. The final response can be obtained using Equation (6): ${}^{FR\_1}_{0}p_i = {}^{1}_{0}\bar{p} + \sum_{h=1}^{H}\left({}^{1}_{0}\tilde{p}_{i,h}\right)$ and ${}_{1}p_i = Re\left\{{}^{FR\_1}_{1}p_i\right\}$ in real values.

If there is more than one excitation, the total response to all excitations will be the summation of different responses due to different excitations by superposition (based on the assumption of that we have a linear system).

Thermal response in complex frequency domain

Complex frequency transfer functions were developed for solid bounded by two parallel planes (Carslaw and Jaeger 1959, Kimura 1977) (also called two-port network method (Athienitis et al. 1985)). Using these transfer functions, the oscillatory thermal responses (i.e. two pairs of temperatures and heat fluxes) on the two opposite surfaces of the solid can be easily obtained if any two of the four variables are given, without discretizing the solid. The two given variables are considered as excitations, and represented with complex DFS as described above.

Equation (7) shows the matrix expression for calculating the oscillatory heat flux and temperature at surface $x = 0$ due to excitations on surface $x = l$ of layer n within an assembly. It is important to note that the values in the excitation vector are the oscillations of different harmonics.

$$\begin{bmatrix} {}^{n}_{0}\tilde{T}_{i,h} \\ {}^{n}_{0}\tilde{p}_{i,h} \end{bmatrix} = {}^{n}_{trs}[M]_h \begin{bmatrix} {}^{n}_{l}\tilde{T}_{i,h} \\ {}^{n}_{l}\tilde{p}_{i,h} \end{bmatrix} \tag{7}$$

$$\text{where} \quad {}^{n}_{trs}[M]_h = \begin{bmatrix} \cosh({}^{n}l \cdot \gamma_h) & \frac{\sinh({}^{n}l \cdot \gamma_h)}{{}^{n}k \cdot \gamma_h} \\ {}^{n}k \cdot \gamma_h \sinh({}^{n}l \cdot \gamma_h) & \cosh({}^{n}l \cdot \gamma_h) \end{bmatrix} \tag{8}$$

where, ${}^{n}l$ is the thickness of layer n, and ${}^{n}k$ is the thermal conductivity $(W/m \cdot K)$. $\gamma_h = \sqrt{s_h/{}^{n}\alpha}$, where $s_h = j\omega_f h$, and ${}^{n}\alpha = {}^{n}k/{}^{n}\rho \cdot {}^{n}c$ is the thermal diffusivity of the material (m^2/sec) of layer n.

For a layer that can be considered as purely resistive/conductive (e.g. insulation, air film), the transmission matrix becomes ${}_{trs}[M]_h = \begin{bmatrix} 1 & R \\ 0 & 1 \end{bmatrix}$. For an exterior air film, $R = 1/{}_{cnv}h$.

The use of transmission matrix makes the calculation the heat transfer in multi-layered plate assemblies (e.g. walls and slabs) straight forward - the overall transmission matrix is simply the multiplication of the individual matrix in the order corresponding to their locations in the assembly. The theory is that the temperature of the common surface of two adjacent layers is obvious the same, and the heat flux through the same surface conserves (Carslaw and Jaeger 1959, Pipes 1957). The overall transmission matrix for a N-layer assembly

$${}^{1\leftarrow N}_{trs}[M]_h = {}_{trs}^{1}[M]_h \cdot {}_{trs}^{2}[M]_h \cdot {}_{trs}^{3}[M]_h \ \ \ldots \ \cdot {}_{trs}^{N}[M]_h \tag{9}$$

where left-hand-side superscript "$1 \leftarrow N$" indicates this transmission matrix is for the assembly from layer 1 to layer N, and the temperature and heat flux on surface l of layer N are the excitations.

The overall admittance matrix needs to be obtained by rewriting (i.e. switch the elements in the excitation and response vectors) the overall transmission matrix:

$$\text{Let} \quad {}^{1\leftarrow N}_{trs}[M]_h = \begin{bmatrix} A_h & B_h \\ C_h & D_h \end{bmatrix} \quad \text{and} \quad {}^{1\leftarrow N}_{adm}[M]_h = \begin{bmatrix} a_h & b_h \\ c_h & d_h \end{bmatrix}$$

Then $a_h = D_h/B_h;\ b_h = C_h - A_h D_h/B_h = -1/B_h;\ c_h = 1/B_h;\ d_h = -A_h/B_h$

For an assembly consisting of N layers of material, the matrix expression for calculating the oscillatory heat flux and temperature at surface 0 of layer 1 due to excitations on surface l of layer N is Equation (10). If the oscillatory temperature excitations on two opposite surfaces are given, the oscillatory heat flow responses on these two surfaces can be obtained with Equation (11). For other combinations of excitations, different matrices need to be derived (Stephenson and Mitalas 1971).

$$\begin{bmatrix} {}^{1}_{0}\tilde{T}_{i,h} \\ {}^{1}_{0}\tilde{p}_{i,h} \end{bmatrix} = {}^{1\leftarrow N}_{trs}[M]_h \begin{bmatrix} {}^{N}_{l}\tilde{T}_{i,h} \\ {}^{N}_{l}\tilde{p}_{i,h} \end{bmatrix} \tag{10}$$

$$\begin{bmatrix} {}^{1}_{0}\tilde{p}_{i,h} \\ {}^{N}_{l}\tilde{p}_{i,h} \end{bmatrix} = {}^{1\leftarrow N}_{adm}[M]_h \begin{bmatrix} {}^{1}_{0}\tilde{T}_{i,h} \\ {}^{N}_{l}\tilde{T}_{i,h} \end{bmatrix} \tag{11}$$

Note the sign conventions in the transmission and admittance matrices are different in the literature. In this paper, the formulation of admittance matrices defines that heat flux p is positive if it flows in the direction pointing from surface at $x = 0$ to surface at $x = l$. For example, negative ${}^{n}_{0}p_i$ means at time i, heat at surface 0 is flowing in the direction pointing from surface l to surface 0 at layer n. At the same time, ${}^{n}_{l}p_i$ can also be positive if heat is being released from the center of layer n.

Treatment of heat sources

To ease the FR analysis of a N-layer wall/floor/ceiling, heat source that are not located at the two outermost nodes of the assembly (Figure 2) can be converted to equivalent temperature potential or heat flow that can be added to those originally located at the two nodes. Alternatively, the assembly and the heat source can be split into two parts that after the split are thermally linked only with the temperature difference of the two nodes. These two approaches will be described in the coming two sub-sections. In this paper, the two outermost nodes, such as the room air node and soil node shown in Figure 1 , are labeled as 0 and L. The heat sources include the transmitted solar radiation absorbed by the slab top surface, heat flux from heat transfer fluid in the channels, and electrical wires that are embedded in the slab

Thévenin theorems for heat sources transformation

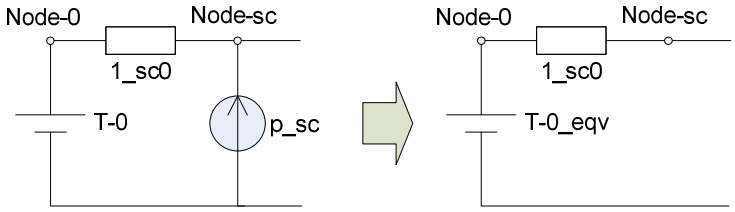

Figure 2: Transformation of thermal network (node 0 is the outer surface of assembly "1 ← sc0", while heat source node sc is at opposite surface of the assembly)

Heat flux can be converted to equivalent temperature potential using Thévenin theorem from electrical circuit network theory. The conversion is similar to process of obtaining the solar-air temperature (ASHRAE 2009) which is commonly used in building simulation and design. Equation (12) can be used to calculate the oscillatory part of the potential. See Figure 2 for network illustration. The mean value part can be obtained in a similar way. See Equation (9) for the definition of ${}^{1\leftarrow sc0}_{trs}[M]_{h_{1,2}}$. If a purely resistive layer laid between node 1 and source node (i.e. Node-sc), ${}^{1\leftarrow sc0}_{trs}[M]_{h_{1,2}}$ equals to the resistance of this layer.

$$_{eqv\_0}^{1}\tilde{T}_{i,h} = {}_{sc}\tilde{p}_{i,h} \cdot {}_{trs}^{1\leftarrow sc0}[M]_{h_{1,2}} + {}_{0}^{1}\tilde{T}_{i,h} \tag{12}$$

Y-diakoptic method and heat flow division

In ventilated BITES systems, the activation of the air flow (i.e. fan on-off) depends on the temperatures of the available inlet air and the system itself. Generally, the air flow is activated if the temperature of the inlet air is certain degrees higher that of the BITES system. Furthermore, the heat exchange between the air flow and the system depends on the temperature difference between the air flow and the air channel surface. Therefore, the temperature of the channel surface is desired for the above two purposes.

Since the slab capacitance is common to its two outermost surface nodes with time-varying temperature, assigning the heat flux from air into these two nodes needs special treatment. Athienitis et al. (1985) applied Y-diakoptic method (Y represents admittance) in the transformation of a wall, which is common to two dynamic thermal zones, into two self-admittances and one transfer-admittance. After this transformation, each original wall surface is connected to one equivalent self-admittance $_{eqv\_slf\_0}^{1\leftarrow sc0}Y_h$ and an equivalent heat source (node 0 from Figure 2 is used as the outermost node for demonstration). The heat source is the product of the equivalent transfer-admittance $_{eqv\_trf\_0}^{1\leftarrow sc0}Y_h$ and the temperature difference between the two wall surfaces. In this case, the internal heat sources are split into two external sources, and the two original wall surfaces can be treated separately.

$$_{eqv\_trf\_0}^{1\leftarrow sc0}Y_h = {}_{adm}^{1\leftarrow N}[M]_{h_{1,2}} \tag{13}$$

$$_{eqv\_slf\_0}^{1\leftarrow sc0}Y_h = {}_{adm}^{1\leftarrow N}[M]_{h_{1,1}} + {}_{adm}^{1\leftarrow N}[M]_{h_{1,2}} \tag{14}$$

For FR analysis on (b) type of ventilated building components, the component is divided into two parts at the level where the heat sources is located. The equivalent admittances of each part can be determined with Y-diakoptic method. The process of obtaining the heat flux from the air flow $_{sc}^{FR}p_i$ is iterative. With an initial guess value of the channel surface, the heat flux $_{sc}p_i$ in real value can be calculated when the temperature of the air flow is high enough for its activation. When there is no flow, the heat flux is zero. In each iteration, the heat flux from the air flow is also represented with complex DFS. The heat flux from the air flow is divided into two portions for the two outermost nodes using current division (Bird 2007). The total heat flux into node 1 is then calculated using Equation (15). After that, the outermost node temperature can be calculated from heat balance at that node. With the known heat flux and temperature of the outermost node, the channel surface temperature can then be updated (Equation (16)). For the oscillatory part of the total heat flow to node 0:

$$\begin{aligned} {}_{0}^{1}\tilde{p}_{i,h} = {}_{eqv\_slf\_0}^{1\leftarrow sc0}Y_h \cdot {}_{eqv\_0}^{1}\tilde{T}_{i,h} + {}_{eqv\_trf\_0}^{1\leftarrow sc0}Y_h \cdot \left({}_{eqv\_L}^{N}\tilde{T}_{i,h} - {}_{eqv\_0}^{1}\tilde{T}_{i,h}\right) \\ + \frac{{}_{trs}^{scN\leftarrow N}[M]_{h_{1,2}}}{-\left({}_{trs}^{1\leftarrow N}[M]_{h_{1,2}}\right)} {}_{sc}\tilde{p}_{i,h} \end{aligned} \tag{15}$$

where $_{eqv\_L}^{N}\tilde{T}_{i,h}$ represents equivalent oscillatory temperature of the other outermost node L on the opposite side of assembly "$1 \leftarrow N$".

$$\begin{bmatrix} {}_{sc}\tilde{T}_{i,h} \\ {}_{sc}\tilde{p}_{i,h} \end{bmatrix} = {}_{trs}^{sc0\leftarrow 1}[M]_h \begin{bmatrix} {}_{eqv\_0}^{1}\tilde{T}_{i,h} \\ {}_{0}^{1}\tilde{p}_{i,h} \end{bmatrix} \tag{16}$$

The final heat flux into node 0 in complex frequency form $_{0}^{FR}p_i = {}_{0}\bar{p} + \sum_{h=1}^{H}\left({}_{0}\tilde{p}_{i,h}\right)$.

3 Numerical models comparison

The two kinds of VCS are analyzed in this paper (Figure 1). Their cross sections are transformed into the two equivalent cross sections shown in Figure 3 by removing the space for the air channels. The transformed cross sections have the same cross section area as the original ones. Treatments of the effective capacitance of radial cross section are given by (Barton et al. 2002, Ren and Wright 1998). Figure 3 also shows the thermal networks of these two kinds of VCS. In the FD approach, two discretization schemes are applied to VCS-a in Figure 3 – the multi-layer dense discretization scheme and 2-layer scheme. The number of layers in the multi-layer scheme depends on the thickness of the slab and the chosen value of the Biot number (0.05 is chosen in this study). For VCS-b, 3-layer scheme is applied based on the study of the discretization schemes for VCS-a. The source-level node is located at the center level of the air channels in the original cross section. The air channels do not have to be at the center of the cross section.

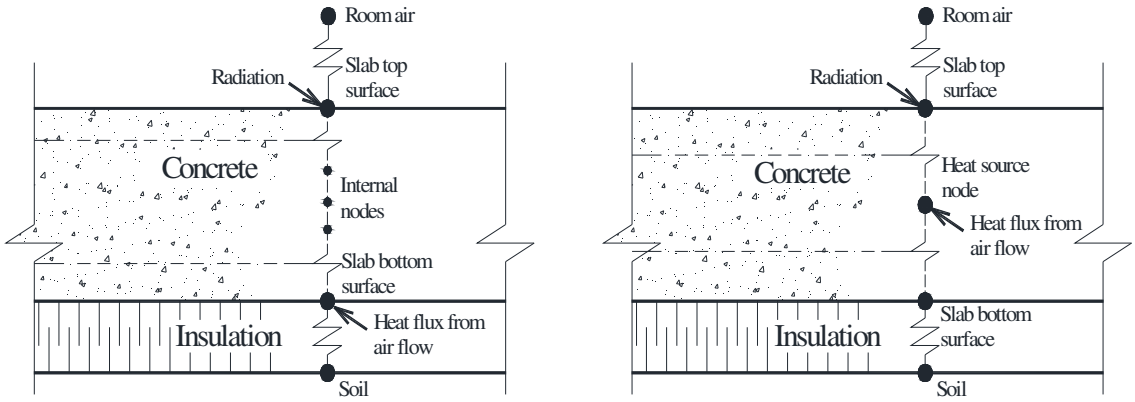

Figure 3: Thermal networks of the two kinds of VCS (Figure 1) after transformation

An iteration technique is applied in solving the heat balance equations. Previously guessed/calculated surface temperature can be used to calculate the heat injection from the air flow. The surface temperature in the next iteration is updated after solving the heat balance equations in the slab for current iteration. This procedure is repeated until convergence criteria are satisfied. For VCS-a, the treatment of the heat flux from the air flow uses the Thévenin theorem transforming method, while, Y-diakoptic method is for VCS-a.

The developed FD models can be subject to periodic and non-periodic excitations, while the FR mode is used under periodic excitations. When the models are subject to periodic excitation, initial conditions are not needed. The thermal response of the slabs can be obtained through iteration. In each iteration, the temperature of the air channel surface is updated, so is the heat flux from the air flow.

Figure 4 shows the selected excitation profiles for the analysis. Soil temperature is set at 11 °C. The flow rate for the hot air flow is 0.2 m^3/sec if the fan is activated. The simulation periods are chosen to be one day (the first day) and two days. The thermo-physical properties of concrete are assumed as follows: specific heat is 840 J/kg/K; density is 2200 kg/m^3; conductivity is 1.7 W/m/K. The conductance of the insulation is 0.5 W/ m^2/K. The surface dimensions of the slab are assumed to be 10 meters long and 3 meters wide.

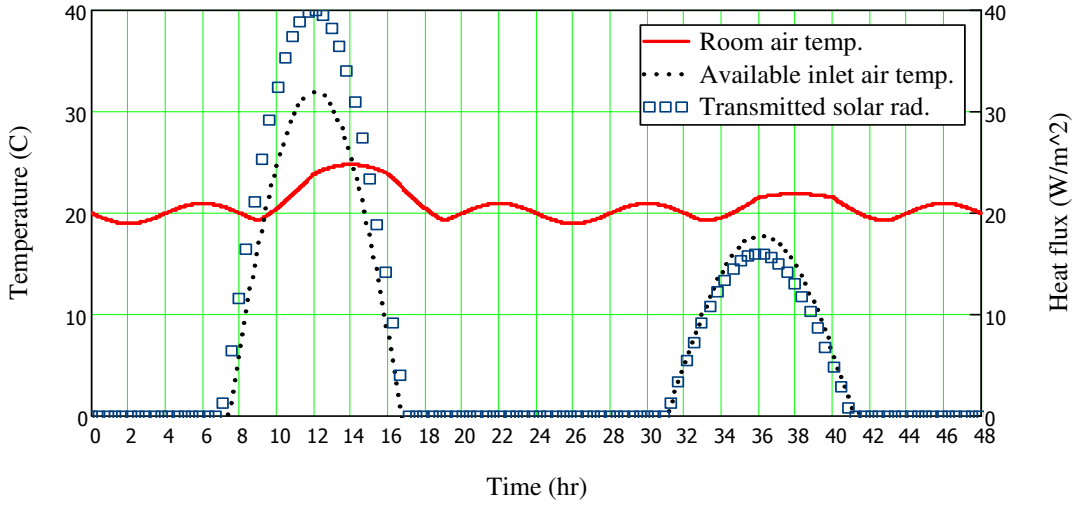

Figure 4: Artificial excitation profiles

Modeling comparison for VCS-a

Simulation results for (a) type of VCS are first compared between a multi-layered FD model and the FR model with 60-second time step. After that the simulation results for the FD model with different discretization schemes and time steps are compared. At the end of the sub-section, the simulation results from a 2-layer FD model are compared with experimental data. Figure 5 shows the simulation results from both FD and FR models for VCS-a. 10 harmonics are used in the FR models. The simulation profiles are close to each other – the maximum temperature difference is 0.6 °C for the bottom surface of the slab. This closeness is also shown under dramatized excitations (i.e. the mean values and amplitudes of excitation are magnified to extreme values).

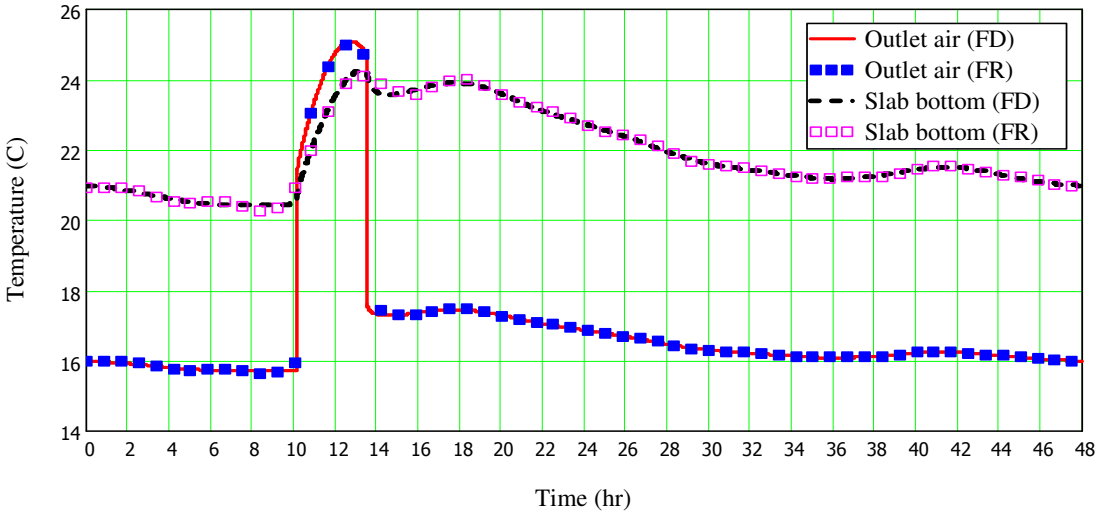

Figure 5: multi-layer FD model vs. FR model (time step of 60 seconds, effective slab thickness of 0.2 m)

Simulation results for the FD model with different discretization schemes and time steps are compared. Comparison shows that 2-layer discretization scheme with time step of half an hour is adequate for providing satisfactory accuracy. The differences between them and the FR modeling results with 60-second time step are less than 5% of the FR results. Fur-

thermore, the difference is reduced as simulation period becomes longer. For FR models, time step of 1 hour is sufficient in providing results with acceptable accuracy. The differences are less than 2% as compared to the simulations with 60-second time step.

FD mode with 2-layer discretization scheme is used to simulate the thermal behavior of an (a) type VCS which is constructed and in use. The VCS slab is located at the basement of an energy-efficient solar house "EcoTerra", which has annual energy consumption about 10% of typical home (Chen et al. 2010b, Doiron et al. 2011). The hot air is supplied from solar air collector (Chen et al. 2010a). The data from one day of slab heating operation is compared with the 2-layer FD model. Figure 6 shows the measured excitation profiles. The curve "Flow rate on/off" in the figure is only an indicator of whether there is flow. The surface-area-weighted heat transfer coefficients $_{eqv\_chn}u_s$ from the air to the slab and to the soil are derived using Equation (1). The heat flux from air flow to the slab and to the soil is calculated based on measured data (Chen et al. 2010a). The measured values are used as the initial boundary conditions for the FD model. The time step for this simulation is 180 seconds, which matches the measurement time interval.

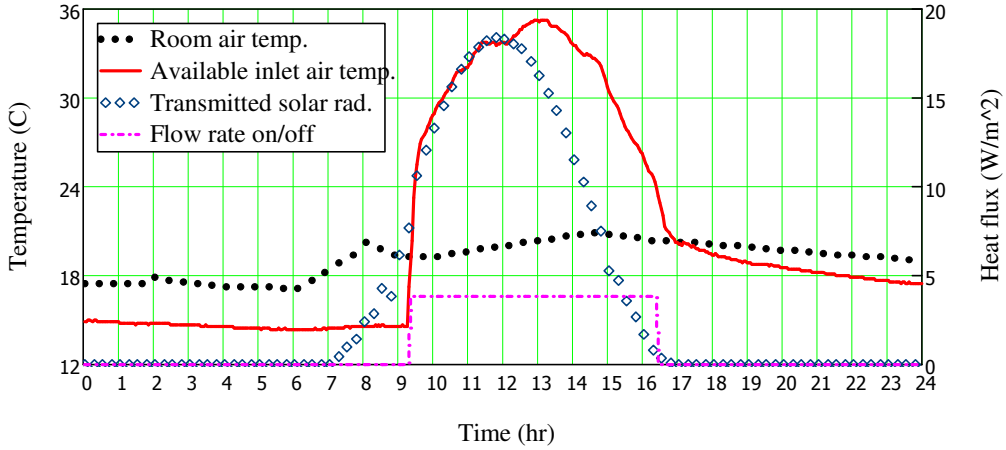

Figure 6: Measured excitation profiles

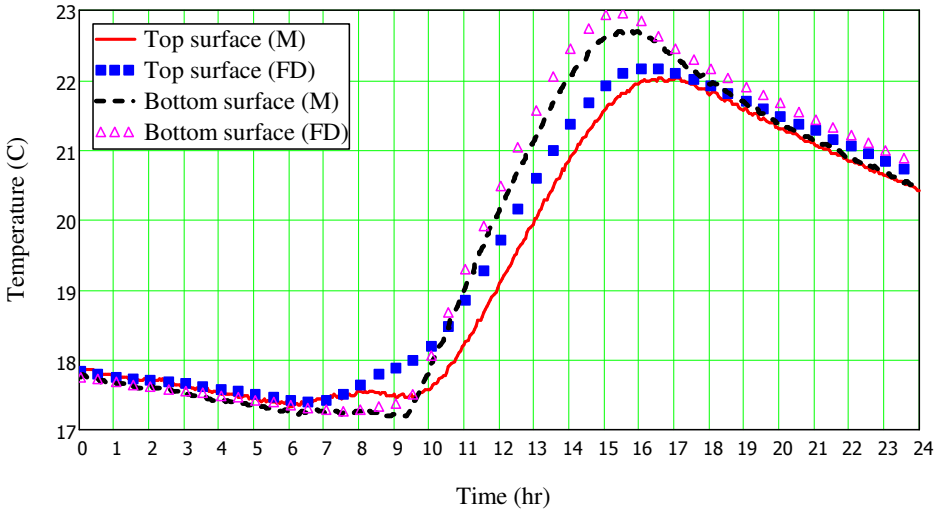

Figure 7: Measured and simulated response profiles for VCS-a

Figure 7 shows the measured and simulated thermal response of the slab. The simulated top and bottom surface temperature profiles match well with the measurement, but with

obvious discrepancy. The largest difference is at 9 am, where the top surface temperature is about 0.6 °C higher than that of the measurement. This discrepancy directly results in the following discrepancy during the slab heating operation (i.e. when air is flowing). There are several potential causes for this discrepancy. The first one is that the measured room air temperature (Figure 6) does not reflect the exact value of the average temperature of the room air and the interior surfaces with which the top surface of the slab exchanged heat in the model. The thermocouple for the room air is located 1.1 meters above the slab on an interior partition. From 6:30 am to 8:30 am, the space heating by forced air system was on. The measurement could have been affected by the supply air temperature. The simulated heat transfer from the room air to the slab top surface becomes larger than actual value. Second cause may be that the thermocouple is not located exactly at the top surface of the slab. It could be up to a centimeter lower than the top surface. Other causes include the imperfect modeling of the boundary condition, such as the heat loss around the edge of the VCS and the CHTC between the slab top surface and the room air. See discussion section for treatment of temperature-dependent CHTC. Nevertheless, the simulation result does not significantly differ from the measurement. The thermal energy changes in the slab between 10 am to 4 pm are 9.55 kWh by simulation, and 9.92 kWh based the average values of the measured slab temperatures. The difference percentage is 4% of the measured value.

FR analysis is not compared with the measurement because the excitation profiles are not periodic. However, the comparison between the FR and FD models indicates that the developed FR model is capable of providing reliable simulation results.

Modeling comparison for VCS-b

Based on the above investigation, it can be concluded that lumped-parameter FR and FD models with time step up to an hour can still provide satisfying results. Hence, thermal models for (b) type of VCS are created using time step of half an hour time. 3-layer discretization scheme (Figure 3) is used for the FD model. Figure 8 shows the comparison of the simulation results under the excitations shown in Figure 4. Total heat flux from air to slab is 7.65 kWh for the FR model and 7.83 kWh for the FD model. The maximum temperature difference is 0.3 °C for the source level of the slab, and 0.3 °C for the outlet air. These two models provide similar results. This indicates that the modeling techniques (i.e. Y-diakoptic method, heat flux division, and iteration procedure) of the FR model are successful and reliable.

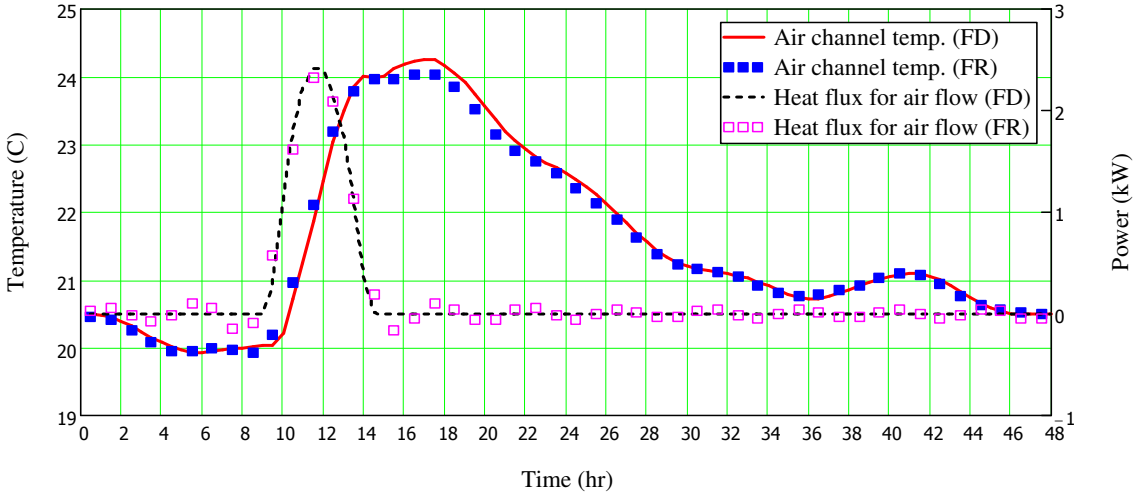

Figure 8: 3-layer FD model vs. FR model (time step of 1800 seconds, effective slab thickness of 0.2 m)

4 Conclusion

Numerical lumped-parameter models for frequency response (FR) and finite difference (FD) analysis have been developed in this paper for ventilated building-integrated thermal energy storage (BITES) systems. Useful modeling techniques, such as heat source transformation with Thévenin theorems and Y-diakoptic method, and heat flow division are presented. Analysis of VCS is used for the demonstration of the modeling techniques. The techniques are applicable to other ventilated BITES systems.

In this paper, discrete Fourier series (DFS) in complex frequency form are used to represent the boundary excitations, such as the surface temperature variation and heat flux associated with air flow. Since the heat conduction equations are also solved in complex frequency domain, this representation is simple and efficient. Modeling results can also be readily transformed to the time domain.

FR and explicit FD modeling are applied to two kinds of VCS – one has air channel on one side of the slab while the other kind has hollow cores as air channel. The relative error introduced by lumped-parameter with large time step has been quantified. 2- or 3-layer discretization schemes with time-step of half an hour can provide satisfactory results. Comparison shows that the simulation results from the lumped-parameter models differ less than 5% of that from FR models with 1-min time step. These models are compared with experimental data. Furthermore, FD models are useful for validating FR models, and vice versa.

5 Acknowledgements

The work is funded by Postgraduate Scholarship from Natural Sciences and Engineering Research Council (NSERC) of Canada and Graduate Student Support Program (GSSP) from Faculty of Engineering and Computer Science (ENCS) of Concordia University, Canada.

6 Nomenclature

j	Imaginary unit; $j = \sqrt{-1}$
p	Power
$Re()$	the real part of the complex number.
t	Time
T	Temperature
ω_h	Angular frequency of the h^{th} harmonic; $\omega_h = 2\pi \cdot h/P$. When $h = 1$, it becomes the fundamental angular frequency ω_f
${}^{1\leftarrow N}_{adm}[M]_h$	Admittance matrix of the h^{th} harmonic for an assembly composed of layers 1 to N.
${}_{eqv\_0}{}^{1}\tilde{T}_{i,h}$	Equivalent oscillatory temperature of surface at $x = 0$ of layer 1 at time i and of h^{th} harmonic
${}^{n}_{0}\tilde{p}_{i,h}/{}^{n}_{l}\tilde{p}_{i,h}$	Oscillatory heat flow of surface at $x = 0\ or\ l$ of layer n at time i and of the h^{th} harmonic
${}_{eqv\_chn}u_s$	Surface-area-weighted heat transfer coefficient of surface s
${}_{mean\_air}T$	Mean air flow temperature

Acronyms

BITES	Building-integrated thermal energy storage
CHTC	Convective heat transfer coefficient

CV/CVs	Control volume(s)
DFS	Discrete Fourier series
FD	Finite difference
FR	Frequency response
VCS	Ventilated concrete slab

Subscripts and superscript

LHS subscripts:

adm	Admittance
sc	Source
slb	Slab
trs	Transmission

LHS superscripts:

$1 \leftarrow N$	Assembly from layer 1 to N
DFS	Discrete Fourier series representation
FR	Complex frequency response

RHS subscripts:

h	Index of harmonic
i	Index of time (time-dependent values are given in discrete form in this paper)
s	Index of surface

7 References

Akander, J. 2000. *The ORC method: Effective modelling of thermal performance of multilayer building components.* Dr.Techn. C804980, Kungliga Tekniska Hogskolan (Sweden).

ASHRAE. 2009. Non-residential cooling and heating load calculations. *ASHRAE Handbook - Fundamentals.* SI ed. Atlanta, GA, USA: American Society of Heating, Refrigerating, and Air-Conditioning Engineers (ASHRAE).

Athienitis, A. K. 1994. *Building Thermal Analysis,* Boston, MA, USA, MathSoft Inc.

Athienitis, A. K., M. Chandrashekar and H. F. Sullivan. 1985. Modelling and analysis of thermal networks through subnetworks for multizone passive solar buildings. *Applied Mathematical Modelling,* 9(2): 109-16.

Athienitis, A. K., M. Stylianou and J. Shou. 1990. A methodology for building thermal dynamics studies and control applications. *ASHRAE Transactions,* 96(2): 839-848.

Athienitis, A. K., H. F. Sullivan and K. G. T. Hollands. 1987. Discrete Fourier-Series Models for Building Auxiliary Energy Loads Based on Network Formulation Techniques. *Solar Energy,* 39(3): 203-210.

Balcomb, J. D. and R. W. Jones. 1983. Passive solar design analysis. *In:* Los Alamos National Laboratory, ed. *Passive Solar Design Handbook.* Boulder, US: American Solar Energy Society.

Barton, P., C. B. Beggs and P. A. Sleigh. 2002. A theoretical study of the thermal performance of the TermoDeck hollow core slab system. *Applied Thermal Engineering,* 22(13): 1485-1499.

Bird, J. O. 2007. *Electrical circuit theory and technology,* Boston, US, Newnes.

Braham, G. D. 2000. Mechanical ventilation and fabric thermal storage. *Indoor and Built Environment,* 9(2): 102-110.

Carslaw, H. S. and J. C. Jaeger. 1959. *Conduction of heat in solids,* Oxford,, Clarendon Press.

Charron, R. and A. K. Athienitis. 2006. Optimization of the performance of double-facades with integrated photovoltaic panels and motorized blinds. *Solar Energy,* 80(5): 482-491.

Chen, W.-K. 1983. *Linear networks and systems,* Monterey, Ca, US, Brooks/Cole Engineering Division.

Chen, Y., A. K. Athienitis and K. Galal. 2010a. Modeling, design and thermal performance of a BIPV/T system thermally coupled with a ventilated concrete slab in a low energy solar house: Part 1, BIPV/T system and house energy concept. *Solar Energy,* 84(11): 1892-1907.

Chen, Y., K. Galal and A. K. Athienitis. 2010b. Modeling, design and thermal performance of a BIPV/T system thermally coupled with a ventilated concrete slab in a low energy solar house: Part 2, ventilated concrete slab. *Solar Energy,* 84(11): 1908-1919.

Davies, M. G. 1982. Optimal RC networks for walls. *Applied Mathematical Modelling,* 6(5): 403-404.

Dincer, I. 2002. On thermal energy storage systems and applications in buildings. *Energy and Buildings,* 34(4): 377-388.

Doiron, M., W. O'Brien and A. Athienitis. 2011. Energy performance, comfort, and lessons learned from a near net zero energy solar house. *ASHRAE Transactions,* 117(2): 585-596.

Fraisse, G., K. Johannes, V. Trillat-Berdal and G. Achard. 2006. The use of a heavy internal wall with a ventilated air gap to store solar energy and improve summer comfort in timber frame houses. *Energy and Buildings,* 38(4): 293-302.

Howard, B. D. 1986. Air core systems for passive and hybrid energy-conserving buildings. *ASHRAE Transactions,* 92(2): p 815-830.

Howard, B. D. and H. Fraker. 1990. Thermal energy storage in building interiors. *In:* B. Anderson, ed. *Solar Building Architecture.* Cambridge, MA, USA: MIT press.

Kimura, K.-I. 1977. Unsteady state heat conduction through walls and slabs. *In:* K.-I. Kimura, ed. *Scientific basis for air-conditioning.* London, UK: Applied Science Publishers Ltd.

Kreyszig, E. 2006. *Advanced engineering mathematics,* Hoboken, NJ, John Wiley.

Morgan, S. and M. Krarti. 2007. Impact of electricity rate structures on energy cost savings of pre-cooling controls for office buildings. *Building and Environment,* 42(8): 2810-2818.

Pipes, L. A. 1957. Matrix analysis of heat transfer problems. *Journal of the Franklin Institute,* 263(3): 195-206.

Ren, M. J. and J. A. Wright. 1998. A ventilated slab thermal storage system model. *Building and Environment,* 33(1): 43-52.

Schmidt, D. and G. Jóhannesson. 2002. Approach for modelling of hybrid heating and cooling components with optimised RC networks. *Nordic Journal of Building Physics,* 3.

Schmidt, D. and G. Jóhannesson. 2004. Optimised RC Networks Incorporated within Macro-Elements for Modelling Thermally Activated Building Constructions. *Nordic Journal of Building Physics,* 3.

Stephenson, D. G. and G. P. Mitalas. 1971. Calculation of heat conduction transfer functions for multi-layer slabs. *ASHRAE Transactions,* 77(2): 117-126.

Winwood, R., R. Benstead and R. Edwards. 1997. Advanced fabric energy storage III: theoretical analysis and whole-building simulation. *Building Services Engineering Research and Technology,* 18: 17-24.

Zmeureanu, R. and P. Fazio. 1988. Thermal performance of a hollow core concrete floor system for passive cooling. *Building and Environment,* 23(3): 243-252.